Title

Soluto-inertial phenomena: Designing long-range, long-lasting, surface-specific interactions in suspensions

Journal

Proceedings of the National Academy of Sciences of the United States of America, 113(31)

ISSN

0027-8424

Authors

Banerjee, Anirudha
Williams, Ian
Azevedo, Rodrigo Nery
et al.

Publication Date

2016-08-02

DOI

10.1073/pnas.1604743113

Peer reviewed

Soluto-inertial phenomena: Designing long-range, long-lasting, surface-specific interactions in suspensions

Anirudha Banerjee[a], Ian Williams[a], Rodrigo Nery Azevedo[a], Matthew E. Helgeson[a], and Todd M. Squires[a,1]

[a]Department of Chemical Engineering, University of California, Santa Barbara, CA 93106

Edited by Monica Olvera de la Cruz, Northwestern University, Evanston, IL, and approved June 2, 2016 (received for review March 22, 2016)

Equilibrium interactions between particles in aqueous suspensions are limited to distances less than 1 μm. Here, we describe a versatile concept to design and engineer nonequilibrium interactions whose magnitude and direction depends on the surface chemistry of the suspended particles, and whose range may extend over hundreds of microns and last thousands of seconds. The mechanism described here relies on diffusiophoresis, in which suspended particles migrate in response to gradients in solution. Three ingredients are involved: a soluto-inertial "beacon" designed to emit a steady flux of solute over long time scales; suspended particles that migrate in response to the solute flux; and the solute itself, which mediates the interaction. We demonstrate soluto-inertial interactions that extend for nearly half a millimeter and last for tens of minutes, and which are attractive or repulsive, depending on the surface chemistry of the suspended particles. Experiments agree quantitatively with scaling arguments and numerical computations, confirming the basic phenomenon, revealing design strategies, and suggesting a broad set of new possibilities for the manipulation and control of suspended particles.

diffusiophoresis | suspensions | long-range interactions | soluto-inertial | colloid

Colloidal suspensions and emulsions of 10-nm to 10-μm particles play a central role in a wide variety of industrial, technological, biological, and everyday processes. Everyday goods, including shampoos, inks, vaccines, paints, and foodstuffs as well as industrial products such as drilling muds, ceramics, and pesticides, rely fundamentally on stably suspended microparticles for their creation and/or operation. This incredible versatility derives from the extensive variety of properties (e.g., mechanical, optical, and chemical) attainable in suspension through a generic set of physicochemical strategies (1–4). A proper understanding of the stability and dynamics of suspensions in general thus underpins both fundamental science and technological applications.

The properties and performance of suspensions depend preeminently on the effective interactions between particles. The celebrated Derjaguin–Landau–Verwey–Overbeek (DLVO) theory (5–7) balances electrostatic interactions (typically repulsive) between charged colloids—as screened by ions in the surrounding electrolyte—against van der Waals attractions, and successfully predicts the stability, phase behavior, and response of electrostatically stabilized suspensions. Additional (non-DLVO) forces can also be used to stabilize or destabilize colloidal suspensions. Grafted or adsorbed macromolecules provide short-range steric repulsions that stabilize suspended particles against van der Waals-induced flocculation (8–11). By contrast, nonadsorbed macromolecules that remain dispersed in solution introduce entropic depletion attractions whose strength and range is set by the size and concentration of depletants (12, 13). Such depletion interactions scale with thermal energy (k_BT), and thus enable tunable and reversible attractions (14, 15). Clever design of shaped or patterned colloids yields "lock-and-key" colloidal interactions (16, 17) and so-called "colloidal molecules" (18, 19). Grafting ligand-functionalized molecules to colloidal surfaces enables molecular sensing (20, 21), and sophisticated design of colloidal self-assembly (22, 23).

Despite the past century's advances in the understanding, control, and engineering of colloidal forces, the range of colloidal interactions remains fundamentally limited. van der Waals interactions extend for tens of nanometers (24–26). Steric repulsions (24, 27) and depletion attractions (12, 24, 28) are limited by the size of the adsorbed, grafted, or suspended macromolecules, typically in the ∼10- to 100-nm range. Of colloidal interactions, electrostatics have the longest range, yet they are fundamentally limited by the (Debye) length scale over which the surface charge is screened by electrolyte ions (10, 24, 27): The largest possible Debye screening length in room temperature aqueous suspensions is ≤1 μm, and more typically between 1 nm and 100 nm. Longer screening lengths are possible in nonpolar solvents, but control and stabilization of nonaqueous charges and suspensions remains challenging (29–32). Magnetic and hydrodynamic interactions are unscreened and can extend to longer ranges (10, 27) but are essentially indiscriminate and less easily controlled, designed, or tuned. Lastly, defects introduced by particles in liquid crystals give rise to interparticle forces over particle length scales (33, 34), yet they are limited to liquid crystalline materials.

In what follows, we demonstrate a versatile strategy to design and establish nonequilibrium interactions that range over hundreds of microns, persist for tens of minutes, and can be designed to attract or repel suspended colloids, depending on the colloids' surface chemistry. These interactions exploit diffusiophoresis (DP)—the migration of suspended particles and droplets in response to gradients or fluxes of solute (35–38) or solvent ("solvophoresis") (39, 40). Such gradients arise spontaneously around membranes, reactive surfaces, electrodes, dissolving solids, evaporating

Significance

Liquid suspensions of micron-scale particles and drops play a ubiquitous role in a broad spectrum of materials of central importance to modern life. A suite of interactions has long been known and exploited to formulate such suspensions; however, all such interactions act over less than a micron in water—and often much less. Here we present a concept to design and engineer nonequilibrium interactions in suspensions, which are particle surface-dependent, may last for hundreds of seconds, and extend hundreds of times farther than is currently possible. The conceptual versatility of the results presented here suggests new capabilities for manipulating suspensions, sorting particles, and synthesizing novel materials and particles.

Author contributions: T.M.S. designed research; A.B. and R.N.A. performed research; A.B., I.W., and M.E.H. contributed new reagents/analytic tools; A.B. and I.W. analyzed data; and A.B., I.W., and T.M.S. wrote the paper.

The authors declare no conflict of interest.

This article is a PNAS Direct Submission.

[1]To whom correspondence should be addressed. Email: squires@engineering.ucsb.edu.

This article contains supporting information online at www.pnas.org/lookup/suppl/doi:10.1073/pnas.1604743113/-/DCSupplemental.

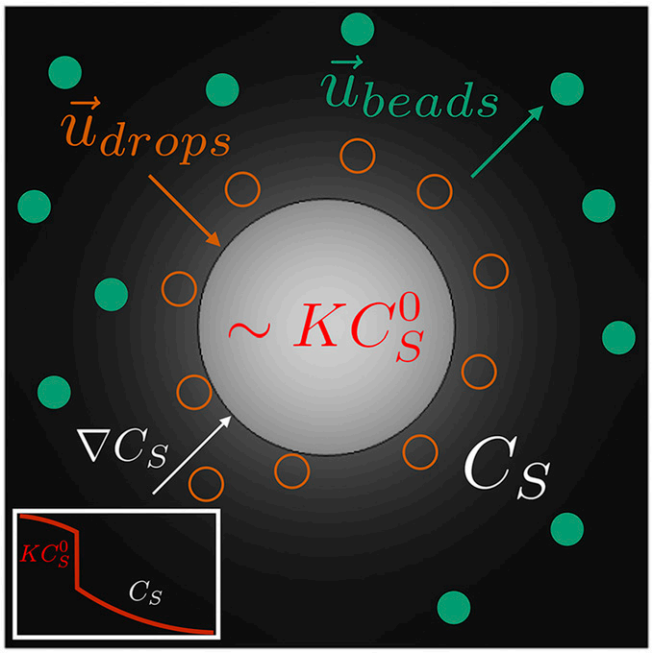

Fig. 1. Long-range SI interactions. An SI beacon (gray), initially loaded with a high solute concentration, is placed in a solute-free suspension. A solute outflux is established during equilibration, driving nearby suspended particles into diffusiophoretic migration. The magnitude and direction of migration depends on interactions between the particle surface and the solute, depicted here by particles of different surface chemistries (orange and green) that migrate either up or down the solute gradient. (*Inset*) Schematic radial profile of solute concentration inside and outside of the beacon.

liquids, or generally in the vicinity of equilibrating surfaces. Recent years have seen a burst of interest in DP in areas ranging from membrane fouling (41), to transport into dead-end pores (42, 43), to self-propelling particles (44–47), to active matter (48–50).

Soluto-Inertial Beacon

Fig. 1 illustrates the mechanism we propose for this interaction, which requires three key ingredients. First, a particle or structure must act as a beacon that generates a long-lasting solute flux. Second are the suspended objects (e.g., colloidal particles, polymers, or emulsion drops), which may be attracted or repelled from the beacon. Third is the solute whose flux mediates the interaction by driving suspended objects into diffusiophoretic migration. Careful choice of these three ingredients (beacon, solute, and suspended particle) enables the duration, direction, and range of the beacon–suspension interactions to be designed and engineered.

Whether the beacon attracts or repels colloids in suspension depends on how those colloids migrate under the chosen solute flux. Theories for diffusiophoretic mobilities involve the relative excess (or depletion) of the solute near the particle surface, which is forced into motion by solute gradients in the bulk solution. Such theories have been developed for gradients of electrolytes (35, 37) and nonelectrolytes (51), yet difficulties in establishing sufficiently strong, stable gradients have prevented systematic experimental measurements (as is routine for electrophoresis). Recent developments in microfluidics, however, have enabled more direct studies of DP (40, 52–56). In particular, we have recently developed a microfluidic device (56) that enables gradients to be directly imposed, and diffusiophoretic migration to be visualized and measured under various solute and solvent gradients (40).

Fig. 2 highlights the surface specificity of DP under a given solute flux. High- and low-concentration SDS solutions flow through the outer "reservoir" channels of a three-channel device, to establish and maintain an SDS gradient of controllable strength across the central sample channel. Even the direction of migration depends on the specific solute/colloid pair. Fluorescent, sulfonated polystyrene (PS) colloids (*Materials and Methods*) move diffusiophoretically down SDS concentration gradients (Fig. 2 *A* and *B*) (Movie S1), consistent with electro-DP (35, 37), treating the (ionic) surfactant SDS as an electrolyte. By contrast, decane drops (*Materials and Methods*) migrate up SDS gradients (Fig. 2 *C* and *D*) (Movie S2), consistent with nonuniform SDS adsorption onto the droplet surface that creates either surface tension gradients, and thus "soluto-capillary" migration (57), or DP under strong adsorption (58). Irrespective of the detailed mechanism at play, a "soluto-inertial" (SI) beacon designed to emit SDS should attract decane droplets but repel PS particles.

Having identified suitable combinations of solute and suspended particles, we now turn to the beacon itself. The beacon must be designed to emit a long-lived solute flux, because the longer the beacon takes to equilibrate with its surrounding solution, the longer the diffusiophoretic interaction lasts. We achieve this long-lived flux by developing the solute analog of "thermal inertia," wherein materials with high volumetric heat capacity resist changes in temperature and thus maintain long-lasting heat flux. SI beacons can be made from materials that strongly partition the solute, so that solute within the beacon (C_B) equilibrates at a concentration that exceeds the concentration in the neighboring solution (C_S) by a large partition coefficient K, giving $C_B = KC_S$, where $K \gg 1$ (59). With such a choice, a beacon loaded with solute that is placed in a solute-free suspension equilibrates over long time scales, as demonstrated and described in *Proof of Principle*, ensuring a long-lived solute outflux (and thus SI interaction). Therefore, the key physicochemical property required of the SI beacon is that it strongly partitions whatever solute has been selected to attract or repel the colloids of interest.

Proof of Principle

Fig. 3 shows proof-of-principle demonstrations of the SI interaction described above, and specifically confirms the range, duration, and particle surface-specificity. Fig. 2 suggests that an SI beacon that emits SDS will repel PS colloids, and attract decane drops. SDS is known to associate with polyethylene glycol (PEG) (60, 61), suggesting that PEG hydrogels will strongly

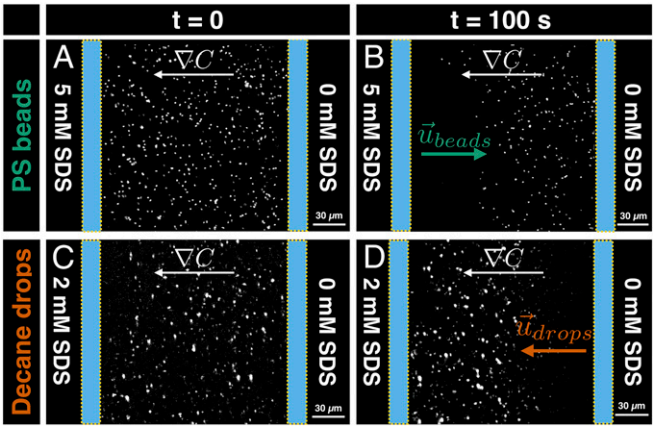

Fig. 2. Particle surface specificity of DP. (*A* and *B*) PS colloids, initially uniformly distributed (*A*), migrate diffusiophoretially down SDS concentration gradients, as seen after 100 s (*B*). (*C* and *D*) By contrast, the DP of fluorescently-dyed decane drops is directed up SDS gradients. In *A* and *C*, $t = 0$ s; in *B* and *D*, $t = 100$ s.

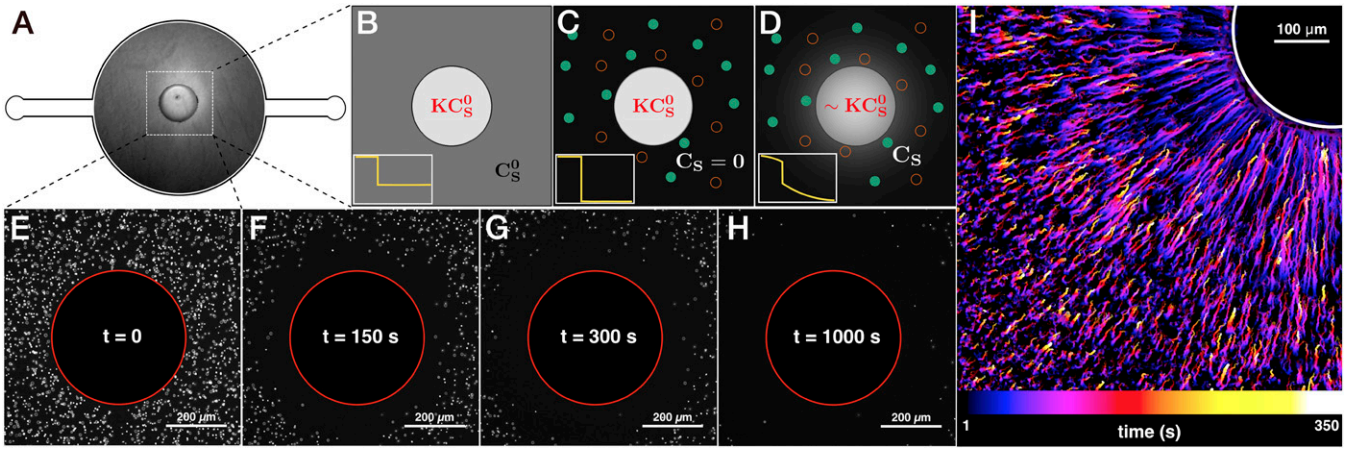

Fig. 3. Experimental demonstration of the range, duration, and particle surface specificity of SI interactions. (*A*) Microfluidic device showing beacon structure (hydrogel post) in the center. (*B*) Loading beacon with solute. (*C*) Flushing loading solution. (*D*) Slow equilibration of stored solute into particle suspension. *Insets* show radial concentration profiles throughout the experiment. (*E–H*) PS particles respond to SDS gradient by migrating over hundreds of microns for tens of minutes: (*E*) $t = 0$ s, (*F*) $t = 150$ s, (*G*) $t = 300$ s, and (*H*) $t = 1{,}000$ s. Beacon location is indicated by red circle. (*I*) Time-stamped streak lines of decane droplet migration in first 350 s of experiment, directed towards the SI beacon. Notably, PS colloids migrate down SDS gradients whereas decane droplets migrate up the SDS gradients.

partition SDS, and thus function as SI beacons. Fig. 3*A* shows a cylindrical SI beacon of radius $R \approx 200$ μm created by photopolymerizing a PEG-diacrylate (PEG-DA) precursor solution in situ within a microfluidic device by exposure to masked, ultraviolet light (56, 62, 63), then flushing unreacted precursor from the device.

The experimental procedure is shown schematically in Fig. 3 *B–D*. An SI beacon is initially loaded by immersion in a 5-mM SDS solution (Fig. 3*B*). The SDS loading solution is then flushed by flowing in a suspension of colloids and/or drops (Fig. 3*C*). The SDS that had partitioned into the SI beacon is no longer in equilibrium with the surrounding solution, and therefore diffuses out of the SI beacon to equilibrate. The resulting SDS concentration gradient persists as long as SDS outfluxes from the SI beacon (Fig. 3*D*), within which suspended colloids and/or drops migrate diffusiophoretically.

Fig. 3 *E–I* reveals this system to behave as predicted: PEG-DA beacons partition SDS, and therefore establish a long-lived, long-ranged SDS flux that effectively repels PS colloids but attracts decane drops. In particular, PS particles are repelled from the SI beacon (down the SDS gradient), forming a 300- to 400-μm-thick particle-free region around the beacon (Movie S3). PS particle migration is evident for at least 1,000 s, by which time most of the particles have migrated out of the microscope field of view. The particle surface specificity of SI interactions is verified by following the same procedure but introducing decane droplets instead of PS colloids. As expected, decane droplets experience a long-range, long-lasting SI attraction toward the beacon, moving up the imposed SDS gradient as shown by the streak lines in Fig. 3*I* and Movie S4. The range and duration in this case is comparable to that observed with PS particles. Notably, the SI interaction range (here 100–1,000 μm) is 10^3–10^4 times larger than the Debye screening length that limits the electrostatic interaction.

SI Model

Having shown that the SI effect can be exploited to generate and direct diffusiophoretic motion in suspensions, we now develop a model of this behavior, focusing initially on spherical SI beacons to avoid the mathematical subtleties of 2D diffusion. A spherical SI beacon is initially loaded by immersion in a loading solution of concentration C_S^0, and thus equilibrates with some beacon concentration $C_B^0 = KC_S^0$. When suspended in a solute-free environment ($C_S = 0$), the solute in the beacon $C_B(t)$ diffuses out into the surrounding solution. We assume that the solute concentration within the beacon evolves rapidly enough that intrabeacon concentration gradients can be neglected [$C_B(r,t) \approx C_B(t)$], and that the concentration within the beacon $C_B(t)$ changes on time scales much slower than are required for $C_S(r,t)$ to evolve. Under these quasi-steady assumptions, the concentration field around a spherical, SI beacon of radius R that partitions solute with a partition coefficient K obeys

$$C_S(r,t) = \frac{C_B(t)}{K}\frac{R}{r}. \quad [1]$$

This concentration field gives rise to a diffusion-limited solute flux $J = 4\pi DRC_B(t)/K$ out of the beacon, where D is the diffusion coefficient of the solute. This outflux must equal the rate at which solute molecules are lost from the beacon,

$$J = \frac{4\pi DRC_B(t)}{K} = -\frac{d}{dt}\left[\frac{4\pi R^3}{3}C_B(t)\right], \quad [2]$$

which can be solved to give the beacon concentration

$$C_B(t) = C_B^0 \exp^{-\frac{3D}{KR^2}t}. \quad [3]$$

Eq. **3** reveals a natural SI time scale,

$$\tau_{SI} = K\frac{R^2}{3D}, \quad [4]$$

over which SI beacons emit solute, which exceeds the diffusion time scale $\tau_D = R^2/D$ by the partition coefficient K, and may thus be many orders of magnitude longer when $K \gg 1$.

We now investigate the range over which colloidal particles migrate diffusiophoretically under the concentration gradient set by the SI beacon. Diffusiophoretic migration velocities under electrolyte gradients are predicted (35, 51) to obey

$$u_{DP} = D_{DP}\nabla \ln C_S, \quad [5]$$

where D_{DP} is the diffusiophoretic mobility of the particle, whose magnitude and sign both depend on the surface chemistry of the particle and solute. Using Eq. **5** for the quasi-steady concentration field around a spherical SI beacon (Eq. **1**) reveals colloids to migrate under a quasi-steady SI outflux with velocity

$$u_{DP}(r) = -\frac{D_{DP}}{r}, \quad [6]$$

decaying with distance like r^{-1}. Several features are notable: The SI migration velocity (*i*) is independent of $C_B(t)$, the instantaneous concentration of solute in the beacon, (*ii*) decays slowly with distance from the SI beacon, and (*iii*) is particle surface-specific, as determined by D_{DP}.

Quantitative Measurements of Migration Velocity

Trajectories of individual particles can be extracted from micrograph series, allowing particle velocities to be measured directly in space and time. Fig. 4 shows raw (*Inset*) and scaled velocity profiles at different times, around cylindrical SI beacons of two different radii (R_P = 130 μm and 200 μm).

No steady-state concentration profile exists for 2D structures like the SI beacons shown in Fig. 3. We therefore solve the transient mass transport problem analytically and numerically using COMSOL Multiphysics, under the same quasi-steady assumptions described in *SI Model*: Concentration fields $C_S(r,t)$ in bulk solution evolve much more rapidly than in the SI beacon (*Supporting Information* and Fig. S1), and so we impose a quasi-steady boundary condition $C_B(t)$. Guided by the scaling arguments for spherical SI beacons, we scale distance by the beacon radius R_P, time by the diffusion time R_P^2/D_{SDS} of dissolved SDS, and concentrations by a concentration scale C_0. In cylindrical coordinates, the nondimensionalized diffusive mass transport equation in the radial direction is given by

$$\frac{\partial \tilde{C}}{\partial \tilde{t}} = \frac{1}{\tilde{r}}\frac{\partial}{\partial \tilde{r}}\left(\tilde{r}\frac{\partial \tilde{C}}{\partial \tilde{r}}\right), \quad [7]$$

where $C_S = C_0\tilde{C}$, $r = R_P\tilde{r}$, and $t = (R_P^2/D_{SDS})\tilde{t}$. The diffusion coefficient D_{SDS} of aqueous SDS below the critical micelle concentration is taken as 780 μm^2/s (64). The concentration field $\tilde{C}(\tilde{r},\tilde{t})$ is then computed by enforcing $\tilde{C}(\tilde{r}=1,\tilde{t}) = 1$ and $d\tilde{C}/d\tilde{r}(\tilde{r}\to\infty,\tilde{t}) \to 0$. The analytical solution (*Supporting Information* and Fig. S2) is in good agreement with the numerical model. The DP migration velocities of suspended particles can then be computed at any position and time from $\tilde{C}(\tilde{r},\tilde{t})$ using Eq. **5**, and are simply proportional to $\nabla \ln \tilde{C}(\tilde{r},\tilde{t})$.

The diffusiophoretic mobility D_{DP} of PS particles under SDS gradients is not known a priori. To compare the measured and calculated SI migration velocities, we normalize all measured or calculated velocities by a single value, corresponding to the maximum value that was measured or calculated,

$$\tilde{u} = \frac{u}{u_{\max}} = \frac{\nabla \ln C_S}{\max|\nabla \ln C_S|}. \quad [8]$$

So long as D_{DP} is constant, normalizing velocities in this way enables direct comparisons between measured and calculated velocity profiles at different times, irrespective of the single (unknown) parameter D_{DP}.

Fig. 4 shows the nondimensional radial velocity profiles of PS colloids measured in experiments with SI beacons of radii R_P = 200 μm (filled blue points) and R_P = 130 μm (empty red points). Each differently colored set of data corresponds to a finite time window, and depict the time evolution of the measured velocity profile around the beacon. Appropriate nondimensionalization allows the experimental data to be compared with the SI model, the predictions from which are plotted as solid lines corresponding to each of the experimental time intervals shown. When properly scaled according to the SI arguments presented above, measured velocity profiles show excellent agreement, in space and time, not only between the two different-sized SI beacons but also between the experimental measurements and the SI model predictions. This collapse justifies our choice of the length, time, and velocity scales as well as confirms that the mass transport model coupled with the quasi-steady state assumption captures the observed SI migration phenomenon quantitatively. It should be noted that, although the velocity profile appears increasingly flat as time progresses, it remains nonzero in both the SI model and the experiment. The success of the scalings for the SI time scale (Eq. **4**) and distance scale R_P, along with the quantitative agreement between theory and experiment in Fig. 4, underscores the quantitative capability to design a long-range, long-lasting suspension interaction.

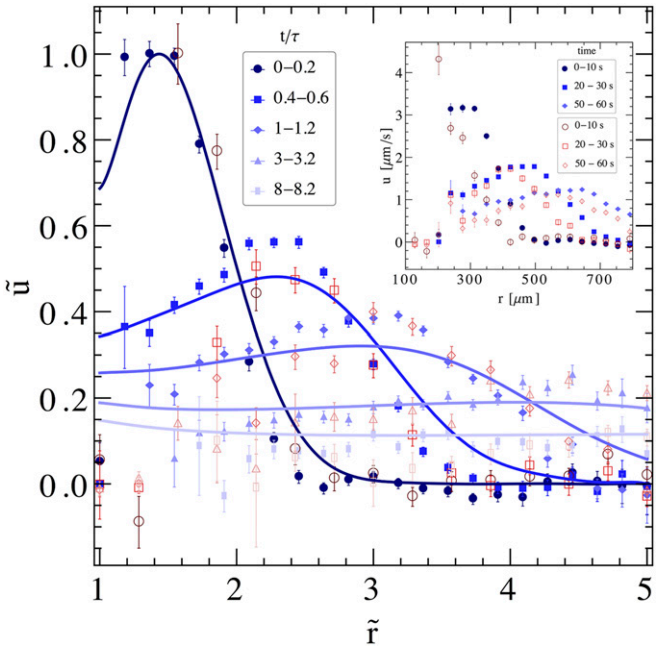

Fig. 4. Radial SI velocity profiles for PS colloids migrating around cylindrical SI beacons of radii R_P = 130 μm (open red symbols) and 200 μm (filled blue symbols), at different times. Points represent data measured in experiment, with unscaled data shown in *Inset*. Scaling distance by post radii R_P, velocities by the maximum velocity $u_{\max}$ measured at any place and time in each experiment, and time by the radial diffusion time R_P^2/D_{SDS} collapses measured data for both posts onto the profiles computed from the quasi-steady mass transport model. Measured and computed velocity profiles at different (scaled) times are represented with different colors, with corresponding t/τ values indicated in the key.

Discussion and Conclusion

The general SI strategy described here shares many features in common with previous observations involving DP, specifically involving reacting or dissolving interfaces. Derjaguin et al. (35) elucidated the existence and influence of DP on latex film formation onto salt-soaked surfaces. Prieve (36) and coworkers noted an analogy with chemically reacting systems, e.g., as steel dissolution drives the diffusiophoretically accelerated deposition of latex particles. More recently, McDermott et al. (65) showed that calcium carbonate particles dissolving in unsaturated aqueous solutions act as diffusioosmotic micropumps, driving flows along neighboring surfaces. Zheng and Pollack (66) reported long-range exclusion near hydrogel boundaries, and Florea et al. (67) revealed ion exchange reactions to form a colloidal exclusion zone near membrane surfaces.

We have established a conceptual framework for the design and engineering of long-range, nonequilibrium interactions in suspension whose magnitude and direction depends on the surface chemistry of the suspended particles. Our results highlight the versatility and generality enabled by combining the slow, SI release of solute with the diffusiophoretic migration of suspended particles. The direction and speed of suspended particle

migration can be controlled by appropriate choice of solute, and the range and duration of the SI interaction can be tuned by choosing size and material of the SI beacon to maximize the partition coefficient. With the specific PEG-DA (beacon)–SDS (solute) system, we have revealed that SI interactions last for tens of minutes and extend over hundreds of microns. Moreover, fairly simple scaling arguments and numerical computations capture the quantitative and qualitative characteristics of SI interactions. Although specific experiments here used relatively large SI beacons held fixed in place, analogous physics and scaling arguments should also hold for freely suspended beacons, although beacon sedimentation introduces additional complexity. The generality of the SI concept naturally suggests a variety of new directions and applications, including the in situ separation and collection of particular suspended colloids, accelerated or triggered flocculation of emulsions and suspensions, layer-by-layer deposition, and other novel synthesis strategies.

Materials and Methods

Device Fabrication. A single inlet/outlet microfluidic device is used, with a large central circular chamber (Fig. 3). A computer-controlled laser cutter (Trotec Speedy 100) cuts the channel into 60-μm-thick scotch tape. The cut tape is then stuck to a Petri dish, which is used as a master for making a polydimethylsiloxane (PDMS) replica of the design. The PDMS master is used to fabricate the device in "microfluidic stickers" (NOA – 81; Norland Adhesive) (68). The central chamber has a radius of 2 mm, and the inlet and outlet channels are 500 μm wide. A glass cover slide is used to seal the device, with holes drilled to provide access for inlet and outlet tubing. A PDMS inlet is ozone-bonded to the cover slide to provide support for inlet and outlet pins and tubings. The device is then baked at 80 °C for at least 4 h to strengthen bonding.

Sample Preparations. SDS solutions are prepared by diluting a 10-mM SDS (Sigma Aldrich) stock solution in deionized water. PEG-DA precursor solution is prepared by mixing 33% (vol/vol) PEG(700)-DA (Sigma-Aldrich) with 4% (vol/vol) photoinitiator (2-hydroxy-2-methylpropiophenone; Sigma-Aldrich) in deionized water; 0.25% vol/vol fluorescent PS beads, 1 μm in diameter (FS03F; Bangs Laboratories), are suspended in clear deionized (DI) water to form the PS suspension. The decane emulsion is prepared by first adding 0.5% vol/vol fluorescent yellow 131SC dye (Keystone) to decane (Sigma Aldrich); 1% vol/vol of the dyed decane is vortexed for 30 s with a 1-mM SDS solution (in DI water) and then sonicated for 15 s to create 1- to 2-μm decane droplets in water.

Experimental Setup. PEG-DA gels are used as SI structures and fabricated using the microscope projection lithography technique (62, 69). A UV lamp is set to 30 mW/cm^2 (measured at an empty objective slot). A 1,000-μm-diameter circular photomask is inserted into the microscope and aligned as described previously (56). PEG-DA precursor solution is injected until the channel is filled. The syringe is disconnected, and 2 min are allowed for flow to relax. Then a 500-ms UV exposure is used with a 10× objective to photopolymerize the gel. The precursor solution is flushed from the device by flowing DI water for 30 min. This results in hydrogel posts of diameter 375–425 μm (Fig. 3). Different sizes of posts are obtained by changing the size of the photomask, the exposure time, and the objective magnification.

Experiments are performed using an inverted microscope (Nikon TE2000U). The hydrogel SI structure is initially loaded with a fixed concentration (5 mM) of SDS, by maintaining flow in the channel for 20 min. SDS solution is then flushed out by displacing with the suspension of PS particles or decane drops. The inlet is pressurized to 500 mbar, and the channel is flushed for 5 s before reducing the pressure to 20 mbar. The focus is adjusted to the center of the channel using a 10× objective. Video recording is started (Andor iXon 885 fluorescence camera) and flow in the channel is stopped using the technique described in ref. 40. In each experiment, images are recorded for 1,000 s at 1 frame per second, with 0.1-s exposure times.

Data Analysis. The 2D particle trajectories are extracted from the fluorescence micrograph series using algorithms adapted from those of Crocker and Grier (70) and implemented in the R programming language, previously used for analysis of bright-field micrographs (71). For each image series, a background image was calculated by finding the time-averaged brightness for each pixel. This background was subtracted from each image in the series. Images were further processed with a spatial band-pass filter and a local background subtraction to eliminate pixel noise and long wavelength brightness fluctuations. This processing has the added benefit of removing out-of-focus particle images, allowing the analysis to focus on particles in the microscope's focal plane. Local brightness maxima are identified as candidate particle positions, and a brightness-weighted centroiding over the particle diameter is performed to obtain particle coordinates with subpixel precision. Finally, trajectories are obtained by linking particle positions between frames in the acquired videos.

The PS particles explore all three dimensions on the timescale of the experiments. However, due to the axisymmetry of the concentration gradient, 2D tracking in the x–y plane is sufficient to observe and explore the diffusiophoretic particle motion. Instantaneous particle velocities in the radial direction are obtained from frame-to-frame displacements, and velocity profiles are calculated by averaging the velocities within annular regions of 50 pixels width with the origin fixed at the center of the beacon. The concentration profile evolves with time and, therefore, so does the velocity profile, and, as such, velocity profiles are calculated independently over 4.5-s (for R_P = 130 μm) and 10-s (for R_P = 200 μm) intervals throughout the experiment. Splitting the experiment into chunks in this way provides more samples in each annular bin, improving the statistics of averaging and suppressing noise in the velocity profiles.

ACKNOWLEDGMENTS. We acknowledge the American Chemical Society Petroleum Research Foundation (Grant 54141-ND5) for primary support of this work. I.W. is supported by the National Institutes of Health under Grant HL-51177, and R.N.A. is supported by the Institute for Collaborative Biotechnologies through Grant W911NF-09-0001 from the US Army Research Office, and by the National Science Foundation (NSF) under Grant CBET-1438779. Work was performed in the University of California Santa Barbara (UCSB) Materials Research Laboratory Central Facilities, a member of the NSF-funded Materials Research Facilities Network, which is supported by the NSF Materials Research Science and Engineering Centers Program under Grant DMR 1121053, and in the UCSB Nanofabrication Facility, a member of the NSF-funded National Nanotechnology Infrastructure Network.

1. Dickinson E (2015) Colloids in food: Ingredients, structure, and stability. *Annu Rev Food Sci Technol* 6:211–233.
2. Joshi YM (2014) Dynamics of colloidal glasses and gels. *Annu Rev Chem Biomol Eng* 5: 181–202.
3. Finne-Wistrand A, Albertsson AC (2006) The use of polymer design in resorbable colloids. *Annu Rev Mater Res* 36:369–395.
4. Zhang J, Luijten E, Granick S (2015) Toward design rules of directional janus colloidal assembly. *Annu Rev Phys Chem* 66:581–600.
5. Derjaguin B, Landau L (1941) Theory of the stability of strongly charged lyophobic sols and of the adhesion of strongly charged particles in solutions of electrolytes. *Acta Physico Chemica URSS* 14:633–662.
6. Verwey EJW (1947) Theory of the stability of lyophobic colloids. *J Phys Colloid Chem* 51(3):631–636.
7. Verwey EJW, Overbeek JTG (1948) *Theory of the Stability of Lyophobic Colloids* (Elsevier, New York).
8. Napper DH (1983) *Polymeric Stabilization of Colloidal Dispersions* (Academic, San Diego).
9. Tadros TF (1991) Steric stabilisation and flocculation by polymers. *Polym J* 23:683–696.
10. Russel W, Saville D, Schowalter W (1989) *Colloidal Dispersions, Cambridge Monographs on Mechanics* (Cambridge Univ Press, Cambridge, UK).
11. Mewis J, Wagner N (2011) *Colloidal Suspension Rheology*, Cambridge Series in Chemical Engineering (Cambridge Univ Press, Cambridge, UK).
12. Asakura S, Oosawa F (1958) Interaction between particles suspended in solutions of macromolecules. *J Polym Sci, Polym Phys Ed* 33(126):183–192.
13. Vrij A (1976) Polymers at interfaces and the interactions in colloidal dispersions. *Pure Appl Chem* 48(4):471–483.
14. Edwards TD, Yang Y, Everett WN, Bevan MA (2015) Reconfigurable multi-scale colloidal assembly on excluded volume patterns. *Sci Rep* 5:13612.
15. Colón-Meléndez L, et al. (2015) Binding kinetics of lock and key colloids. *J Chem Phys* 142(17):174909.
16. Sacanna S, Irvine WTM, Chaikin PM, Pine DJ (2010) Lock and key colloids. *Nature* 464(7288):575–578.
17. Ashton DJ, Jack RL, Wilding NB (2015) Porous liquid phases for indented colloids with depletion interactions. *Phys Rev Lett* 114(23):237801.
18. Teich EG, van Anders G, Klotsa D, Dshemuchadse J, Glotzer SC (2016) Clusters of polyhedra in spherical confinement. *Proc Natl Acad Sci USA* 113(6):E669–E678.
19. Glotzer SC, Solomon MJ (2007) Anisotropy of building blocks and their assembly into complex structures. *Nat Mater* 6(8):557–562.
20. Pregibon DC, Toner M, Doyle PS (2007) Multifunctional encoded particles for high-throughput biomolecule analysis. *Science* 315(5817):1393–1396.
21. Geerts N, Eiser E (2010) DNA-functionalized colloids: Physical properties and applications. *Soft Matter* 6(19):4647–4660.
22. Rogers WB, Crocker JC (2011) Direct measurements of DNA-mediated colloidal interactions and their quantitative modeling. *Proc Natl Acad Sci USA* 108(38): 15687–15692.

23. McGinley JT, Jenkins I, Sinno T, Crocker JC (2013) Assembling colloidal clusters using crystalline templates and reprogrammable DNA interactions. *Soft Matter* 9(38): 9119–9128.
24. Israelachvili JN (2011) *Intermolecular and Surface Forces* (Academic, San Diego), 3rd Ed.
25. Hamaker H (1937) The London–van der Waals attraction between spherical particles. *Physica* 4(10):1058–1072.
26. Lifshitz EM (1956) The theory of molecular attractive forces between solids. *Sov Phys* 2(1):73–83.
27. Ivlev A, Löwen H, Morfill G, Royall CP (2012) *Complex Plasmas and Colloidal Dispersions* (World Scientific, Singapore).
28. Vincent B (1990) The calculation of depletion layer thickness as a function of bulk polymer concentration. *Colloids Surf* 50:241–249.
29. Hsu MF, Dufresne ER, Weitz DA (2005) Charge stabilization in nonpolar solvents. *Langmuir* 21(11):4881–4887.
30. Smith GN, Hallett JE, Eastoe J (2015) Celebrating *Soft Matter*'s 10th anniversary: Influencing the charge of poly(methyl methacrylate) latexes in nonpolar solvents. *Soft Matter* 11(41):8029–8041.
31. Rios de Anda I, Statt A, Turci F, Royall CP (2015) Low-density crystals in charged colloids: Comparison with Yukawa theory. *Contrib Plasma Phys* 55(2-3):172–179.
32. Sainis SK, Germain V, Mejean CO, Dufresne ER (2008) Electrostatic interactions of colloidal particles in nonpolar solvents: Role of surface chemistry and charge control agents. *Langmuir* 24(4):1160–1164.
33. Guzmán O, Kim EB, Grollau S, Abbott NL, de Pablo JJ (2003) Defect structure around two colloids in a liquid crystal. *Phys Rev Lett* 91(23):235507.
34. Koenig GM, Jr, de Pablo JJ, Abbott NL (2009) Characterization of the reversible interaction of pairs of nanoparticles dispersed in nematic liquid crystals. *Langmuir* 25(23):13318–13321.
35. Derjaguin BV, Dukhin SS, Korotkova AA (1993) Diffusiophoresis in electrolyte solutions and its role in the mechanism of the formation of films from caoutchouc latexes by the ionic deposition method. *Prog Surf Sci* 43(20):153–158.
36. Prieve DC (1982) Migration of a colloidal particle in a gradient of electrolyte concentration. *Adv Colloid Interface Sci* 16(1):321–335.
37. Prieve DC, Anderson JL, Ebel JP, Lowell ME (1984) Motion of a particle generated by chemical gradients. Part 2. Electrolytes. *J Fluid Mech* 148:247–269.
38. Anderson JL (1989) Colloid transport by interfacial forces. *Annu Rev Fluid Mech* 21: 61–99.
39. Kosmulski M, Matuevi E (1992) Solvophoresis of latex. *J Colloid Interface Sci* 150(1): 291–294.
40. Paustian JS, et al. (2015) Direct measurements of colloidal solvophoresis under imposed solvent and solute gradients. *Langmuir* 31(15):4402–4410.
41. Kar A, Guha R, Dani N, Velegol D, Kumar M (2014) Particle deposition on microporous membranes can be enhanced or reduced by salt gradients. *Langmuir* 30(3):793–799.
42. Kar A, Chiang TY, Ortiz Rivera I, Sen A, Velegol D (2015) Enhanced transport into and out of dead-end pores. *ACS Nano* 9(1):746–753.
43. Shin S, et al. (2016) Size-dependent control of colloid transport via solute gradients in dead-end channels. *Proc Natl Acad Sci USA* 113(2):257–261.
44. Kline TR, Paxton WF, Mallouk TE, Sen A (2005) Catalytic nanomotors: Remote-controlled autonomous movement of striped metallic nanorods. *Angew Chem Int Ed Engl* 44(5):744–746.
45. Moran JL, Posner JD (2011) Electrokinetic locomotion due to reaction-induced charge auto-electrophoresis. *J Fluid Mech* 680:31–66.
46. Brady JF (2011) Particle motion driven by solute gradients with application to autonomous motion: continuum and colloidal perspectives. *J Fluid Mech* 667:216–259.
47. Golestanian R, Liverpool TB, Ajdari A (2005) Propulsion of a molecular machine by asymmetric distribution of reaction products. *Phys Rev Lett* 94(22):220801.
48. Ibele M, Mallouk TE, Sen A (2009) Schooling behavior of light-powered autonomous micromotors in water. *Angew Chem Int Ed Engl* 48(18):3308–3312.
49. Theurkauff I, Cottin-Bizonne C, Palacci J, Ybert C, Bocquet L (2012) Dynamic clustering in active colloidal suspensions with chemical signaling. *Phys Rev Lett* 108(26):268303.
50. Buttinoni I, Volpe G, Kümmel F, Volpe G, Bechinger C (2012) Active Brownian motion tunable by light. *J Phys Condens Matter* 24(28):284129.
51. Anderson JL, Lowell ME, Prieve DC (1982) Motion of a particle generated by chemical gradients Part 1. Non-electrolytes. *J Fluid Mech* 117:107–121.
52. Abécassis B, Cottin-Bizonne C, Ybert C, Ajdari A, Bocquet L (2008) Boosting migration of large particles by solute contrasts. *Nat Mater* 7(10):785–789.
53. Abécassis B, Cottin-Bizonne C, Ybert C, Ajdari A, Bocquet L (2009) Osmotic manipulation of particles for microfluidic applications. *New J Phys* 11(7):1–21.
54. Palacci J, Abécassis B, Cottin-Bizonne C, Ybert C, Bocquet L (2010) Colloidal motility and pattern formation under rectified diffusiophoresis. *Phys Rev Lett* 104(13):138302.
55. Palacci J, Cottin-Bizonne C, Ybert C, Bocquet L (2012) Osmotic traps for colloids and macromolecules based on logarithmic sensing in salt taxis. *Soft Matter* 8(4):980–994.
56. Paustian JS, Azevedo RN, Lundin STB, Gilkey MJ, Squires TM (2014) Microfluidic microdialysis: Spatiotemporal control over solution microenvironments using integrated hydrogel membrane microwindows. *Phys Rev X* 3:041010.
57. Levich BG, Kuznetsov AM (1962) On the motion of drops in liquids under the action of surface active substances. *Dokl Akad Nauk SSSR* 146(1):145–147.
58. Anderson JL, Prieve DC (1981) Diffusiophoresis caused by gradients of strongly adsorbing solutes. *Langmuir* 7(2):403–406.
59. Leo A, Hansch C, Elkins D (1971) Partition coefficients and their uses. *Chem Rev* 71(6): 525–616.
60. Tam KC, Wyn-Jones E (2006) Insights on polymer surfactant complex structures during the binding of surfactants to polymers as measured by equilibrium and structural techniques. *Chem Soc Rev* 35(8):693–709.
61. Kim J, Gao Y, Hebebrand C, Peirtsegaele E, Helgeson ME (2013) Polymer–surfactant complexation as a generic route to responsive viscoelastic nanoemulsions. *Soft Matter* 9(29):6897–6910.
62. Dendukuri D, Gu SS, Pregibon DC, Hatton TA, Doyle PS (2007) Stop-flow lithography in a microfluidic device. *Lab Chip* 7(7):818–828.
63. Helgeson ME, Chapin SC, Doyle PS (2011) Hydrogel microparticles from lithographic processes: Novel materials for fundamental and applied colloid science. *Curr Opin Colloid Interface Sci* 16(2):106–117.
64. Leaist DO (1986) Binary diffusion of micellar electrolytes. *J Colloid Interface Sci* 111(1): 230–239.
65. McDermott JJ, et al. (2012) Self-generated diffusioosmotic flows from calcium carbonate micropumps. *Langmuir* 28(44):15491–15497.
66. Zheng JM, Pollack GH (2003) Long-range forces extending from polymer-gel surfaces. *Phys Rev E Stat Nonlin Soft Matter Phys* 68(3 Pt 1):031408.
67. Florea D, Musa S, Huyghe JMR, Wyss HM (2014) Long-range repulsion of colloids driven by ion exchange and diffusiophoresis. *Proc Natl Acad Sci USA* 111(18): 6554–6559.
68. Bartolo D, Degré G, Nghe P, Studer V (2008) Microfluidic stickers. *Lab Chip* 8(2): 274–279.
69. Love JC, Wolfe DB, Jacobs HO, Whitesides GM (2001) Microscope projection photolithography for rapid prototyping of masters with micron-scale features for use in soft lithography. *Langmuir* 17(19):6005–6012.
70. Crocker JC, Grier DG (1996) Methods of digital video microscopy for colloidal studies. *J Colloid Interface Sci* 179(1):298–310.
71. Gray AT, Mould E, Royall CP, Williams I (2015) Structural characterisation of polycrystalline colloidal monolayers in the presence of aspherical impurities. *J Phys Condens Matter* 27(19):194108.